2013 European Control Conference (ECC)
July 17-19, 2013, Zürich, Switzerland.

Experimental Validation of Equilibria in Fuel Cells with Dead-Ended Anodes

Jixin Chen, Jason B. Siegel, Toyoaki Matsuura, Anna G. Stefanopoulou and Serhat Yesilyurt

Abstract— **This paper investigates the nitrogen blanketing front during the dead-ended anode (DEA) operation of a PEM fuel cell. It is found that the dynamic evolution of nitrogen accumulation in the DEA of a PEM fuel cell eventually arrives to a steady-state, which suggests the existence of equilibrium. We use a multi-component model of the two-phase, one-dimensional (along-channel) system to analyze this phenomenon. Specifically, the model is first verified with experimental observations, and then utilized to show the evolution toward equilibrium. The full order model is reduced to a second-order partial differential equation (PDE) with one state, which can be used to predict and analyze the observed steady state DEA behavior. The parametric study is performed focusing on the influence of the cathode pressure on the existence of equilibrium in the DEA condition.**

I. Introduction

Dead-end anode (DEA) operation of a PEM fuel cell has been implemented by several groups [1], [2], [3] and applied in a commercial fuel cell module, the Nexa (1.2 KW stack of 42 cells) from Ballard Power Systems [4]. In DEA operation, hydrogen is fed into anode with regulated pressure at the inlet, whereas the cathode is operated with conventional flow-through conditions associated with a stoichiometry ratio (SR) greater than one. Since the Nafion membrane is not an ideal separator, nitrogen and water can diffuse through the membrane from the cathode and accumulate in the anode. In vertically oriented channel as shown in Fig. 1, the reaction drives the convective transport of gas mixture toward the channel end. The accumulation of inert nitrogen at the channel end displaces hydrogen and eventually leads to a starvation at the channel end. The spatial variation of the species in the anode results in uneven local current distribution. The depletion of hydrogen over time leads to the decreasing cell voltage under galvanostatic operation. For example, in our 50 cm^2 DEA cell experiment, the voltage dropped from 0.7 to 0.6 V in about 15 minutes at a constant current load of 0.4 A/cm^2 as shown in Fig. 3 [5].

Purging of the anode is typically needed to release accumulated nitrogen and water and maintain a manageable voltage range. A purge, normally taking 20-900 ms, is implemented by a solenoid valve at the downstream of the anode. Since the anode pressure is regulated at the upstream of anode, the opening of solenoid valve leads to turbulent orifice flow which clears the nitrogen and water from the anode channels. The downstream purge valve and the upstream pressure regulator are the only hardware at the anode side for a DEA system. As a comparison, conventional flow-through anode (FTA) fuel cell system depends on a recirculation loop to maintain a high hydrogen utilization, which requires hydrogen grade plumbing and hardware such as ejector/blower and water separator. These components add weight, volume, and expense to the system.

Funding is provided by the National Science Foundation. The first four authors are with the Fuel Cell Control Laboratory, University Michigan, Ann Arbor, MI 48109, USA. S. Yesilyurt is at Sabanci University, Turkey. Corresponding Email: jixinc@umich.edu (J. Chen)

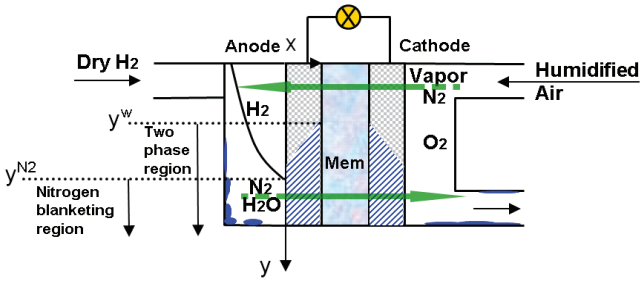

Fig. 1. Equilibrium scenario in DEA operation (not to scale). The net flux of nitrogen is from anode to cathode in the channel end-region, as opposed to other regions. Globally, zero net fluxes of nitrogen and water through the membrane are achieved at equilibrium.

Motivated by the experimental findings of [6], the possibility of operating the DEA cell without purging is analyzed in this paper. We address the conditions under which system equilibrium could be achieved with relatively stable voltage output under galvanostatic operation, and how to obtain a reasonable power under such equilibrium conditions. Voltage equilibrium was indeed observed in prior experimental studies [7], [8]. These findings motivate our further investigation by mechanism analysis and simulation using the validated model.

As shown in Fig. 1, a stratified channel distribution with water and nitrogen in the end can be observed for the DEA cell [3]. In this case the local nitrogen partial pressure may easily exceed the cathode, particularly in the channel end region. The nitrogen diffuses from the anode to the cathode due to the partial pressure gradient as illustrated by the bottom arrow (positive x-direction). In the upper portion of the cell, the nitrogen crossover is from cathode to anode (negative x-direction). The nitrogen continues to accumulate in the anode until a global balance of nitrogen crossover has been achieved, meaning a zero net flux of nitrogen. The nitrogen partial pressure in the anode depends on the rate of crossover and the convective velocity, which are coupled with the current density distribution. An equilibrium for nitrogen blanketing front is necessary for the equilibrium of the whole DEA fuel cell system. There is a non-linear coupling of anode nitrogen partial pressure and membrane hydration which introduces further complexity while analyzing such equilibrium. The local electrochemical reaction rate depends

on the hydrogen concentration, or nitrogen concentration due to the regulated anode pressure, and determines the local water generation rate, which affects the membrane water content. The membrane permeation coefficient for nitrogen, as a function of membrane water content and temperature, in turn influences the local nitrogen crossover rate and the establishment of nitrogen equilibrium.

In previous work [9], the effect of nitrogen accumulation in the anode on the voltage decay has been demonstrated by modeling nitrogen crossover and convective transport. However, the model neglected the impact of diffusion in the anode channel, which can be significant for the deeper channel geometry studied here. A one-dimensional, single-phase and transient model considering both convection and diffusion has been developed [10] to capture the spatiotemporal evolution of species and electrochemical reaction in a DEA cell. The model was further extended to include the cathode carbon corrosion caused by the anode fuel starvation and associated irreversible voltage degradation over time [11]. Recently, the model was improved to be 1+1D (along channel + through membrane) and two-phase so that the purge behavior can be predicted more accurately for an optimization study of purge scheduling [12]. After careful tuning, the present full-order-model can capture comprehensive mass transport and electrochemical processes in DEA operation with satisfactory accuracy. The model can be used for predicting the equilibrium behavior [7]. However, the full-order-model requires numerical tools with substantial computational expense to investigate the equilibrium.

Therefore, we focus on reducing the number of model states. It is anticipated that the reduced-order-model can still predict the equilibrium behavior and characteristics. Similar publications (simulation and analysis) focus on the fuel cell equilibrium from Benziger's group [13], [14], [15], [16]. However, those studies are based on a stirred-tank-reactor (STR) fuel cell. In their case both anode and cathode supplies are dry or slightly humidified to comply with the auto-catalytic concept of the STR fuel cell and the equilibrium arises from a water balance. The effect of convective transport is eliminating by the open channel architecture. Although both STR and DEA cell feature self-humidification and spatial inhomogeneity, the equilibrium behavior in DEA cell represents a more complicated scenario where both diffusion and convection must be considered. The convection leads to the stratified channel distribution of gas species in the vertically oriented cell. The diffusive transport in the channel is equally important by moderating the effect of nitrogen blanketing in the anode channel.

The paper is organized as follows. Since the model has been detailed in prior works [11], [12] a brief overview is provided in this paper. The model validation against the flow-through polarization and DEA operation data will be presented. The tuned model predicts the voltage evolution toward equilibrium in DEA operation, achieving satisfactory agreement with the experimental data. Finally A single-state PDE system based on the nitrogen distribution in the anode is derived. This reduced order model is shown to predict the evolution toward equilibrium and capture the influence of cathode pressure.

II. Model Summary and Validation

The baseline (full-order) model is 1+1D, two-phase and transient, which generally captures all transport phenomena and reaction kinetics in the vertically oriented DEA cell.

The model parameters relevant to the species distribution in the anode have been tuned in prior works [10], [11]. These parameters include the nitrogen permeation scale factor, the oxygen crossover scale factor, and the hydrogen concentration parameter [10], [11]. They are kept unchanged in this paper. Another group of parameters that relate to the cell polarization are further tuned: the exchange current density of oxygen reaction (i_{0,O_2}) and the contact resistance (R_{GDL}). These two parameters influence the reaction kinetics and cell voltage by the Butler-Volmer equation as shown in (1) and (2) with detailed discussions in [11]. The average current density is related to the local current density by (3).

$$i(y,t) = i_{0,O_2}\Big\{\frac{P_{V,CA}}{P^*_{V,CA}}\exp\Big[\frac{\alpha_{a,O_2}F}{RT}(\eta^{CA})\Big] - \left(\frac{P^{CL}_{O_2,CA}}{P^*_{O_2,CA}}\right)^{\beta_{O_2}}\left(\frac{P_{H_2}}{P^*_{H_2}}\right)^{\beta_{H_2}}\exp\Big[\frac{-\alpha_{c,O_2}F}{RT}(\eta^{CA})\Big]\Big\} \quad (1)$$

$$\begin{aligned}\eta^{CA} &= V_m^{CA} - \phi_{CA} - V_{O_2}^{eq} \\ &= V_m^{AN} + E_{cell} + R_{GDL}i_{AN} - \phi_{CA} - V_{O_2}^{eq}\end{aligned} \quad (2)$$

$$i_{fc} = \frac{1}{L}\int_0^L i(y,t)dy \quad (3)$$

TABLE I
Tuned parameters in the model

Quantity	Value	Range
i_{0,O_2}	0.8×10^{-9} A/cm^2	10^{-10}–10^{-8} A/cm^2
R_{GDL}	0.34 Ω cm^2	0.1–0.8 Ω cm^2

Figure 2 shows the polarization performance obtained from the flow-through operation and Figure 3 illustrates the voltage evolution in three continuous DEA cycles for two cases with different cathode supply RH. The DEA model is used to predict flow-through operation by assigning a constant to the flux at the anode outlet N_{out} [12] so that the desired anode SR is achieved. The polarization data in the flow-through condition 1 are used for tuning the model parameters; whereas the polarization performances in the other three conditions and the voltage cycling data under DEA operation in Fig. 3 are used for validation of the tuned model. The tuning was performed based on the least squares algorithm in order to minimize the differences between the experimental and simulation data of cell voltage. The tuned parameter values are shown in Table I.

The model prediction shows satisfactory agreement with the experimental data for flow-through operation. The model

can capture the performance improvement due to the increased cathode pressure and RH, although the difference is limited as the cathode pressure increases from 2 to 10 psig. Under 100% cathode RH and elevated current density conditions, the model over-estimates the voltage probably because the influence of liquid water on the oxygen transport in the cathode channel is not modeled. When the cathode RH has been reduced to 50%, the model prediction is closer to the experimental data at the elevated current densities. The satisfactory agreement at small current densities is important since the model is used for studying DEA operation at low current densities.

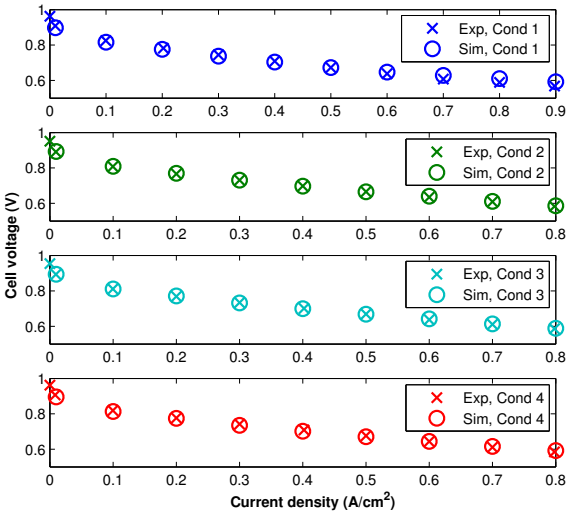

Fig. 2. The comparison of polarization performance between modeling and experimental data for 4 sets of operating conditions. Condition 1: pressure 2.5/2.5 psig and RH 100%/100% for anode/cathode; condition 2: pressure 2/2 psig and RH 100%/50% for anode/cathode; condition 3: pressure 2/4 psig and RH 100%/50% for anode/cathode; condition 4: pressure 2/10 psig and RH 100%/50% for anode/cathode. For all conditions, the cell temperature is 60°C and the stoichiometry ratio is 1.2/2.5 for anode/cathode. The model can predict the polarization performance with satisfactory accuracy.

The tuned model can predict the voltage evolution toward an equilibrium in DEA operation when the purge is disabled, with satisfactory agreement compared to the experimental data. Figure 4 shows two cases that achieved equilibrium in the experiment after approximately 100 minutes of DEA operation, as well as the simulation results with the same operating conditions. The experimental findings shown in Fig. 5 indicate that the cathode pressure needs to be reduced to achieve the equilibrium (2.4 versus 4.0 psig), since large partial pressure of nitrogen could blanket too much area in the anode and shutdown the cell. On the other hand, high cathode RH should be avoided in order to obtain an equilibrium since the liquid accumulation could cause a localized shutdown. In Fig. 5, the equilibrium was achieved with cathode supply RH of 60%. Generally, the humidified cathode supply introduces additional complexity and randomness in DEA equilibrium. For example, the erratic voltage behavior after reaching equilibrium can be attributed

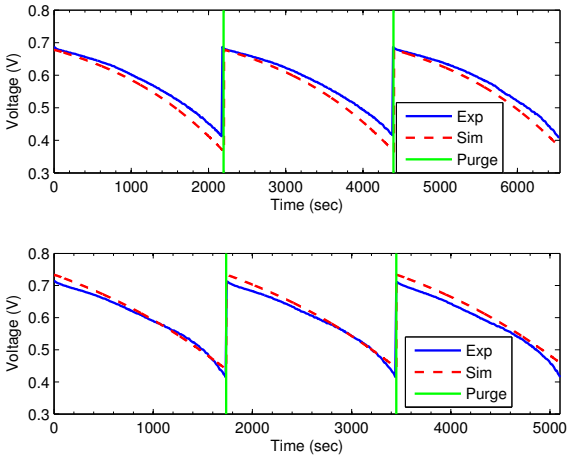

Fig. 3. The comparison of cell voltage evolution within three continuous cycles. The operating conditions are: cell temperature 60 °C, cathode SR 2.5, both anode and cathode pressures 3.8 psig, and current density 0.4 A/cm^2. The cathode supply RH is 50% for the first subplot and 100% for the second one.

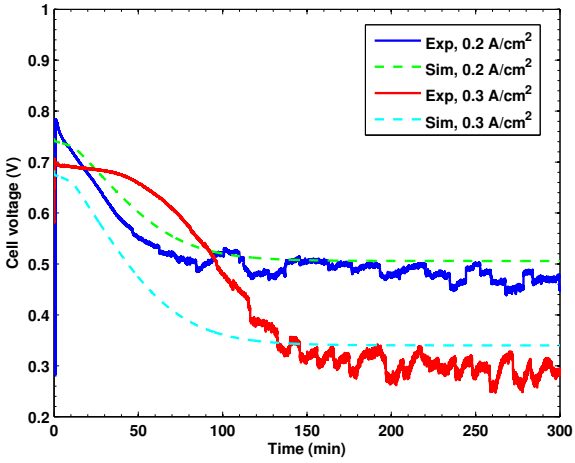

Fig. 4. The model predicted and experimental voltage evolution towards equilibrium in DEA operation. The operating conditions are 65°C cell temperature, 60% cathode supply RH, 4.0/2.4 psig anode/cathode pressure, and 2.5 cathode SR. The equilibria have been reached with current density of 0.2 and 0.3 A/cm^2

to liquid water condensation in the anode channel, which forms droplets that randomly block the channel before falling to the bottom of the channel. In addition, the increased local current in the nitrogen non-blanketing region under equilibrium leads to higher water generation rate in the catalyst layer, which also contributes to the erratic voltage. In Fig. 4, the case with 0.3 A cm^{-2} shows higher magnitude of voltage oscillation compared with 0.2 A cm^{-2}.

III. Reduced Order Modeling

In this section, we analyze the equilibrium behavior using the reduced-order-model (ROM) instead of the full-order-model (FOM) shown in [11], [12]. The validity of reduced order modeling will be examined by a comparison with the FOM simulation. It is expected that the existence of DEA

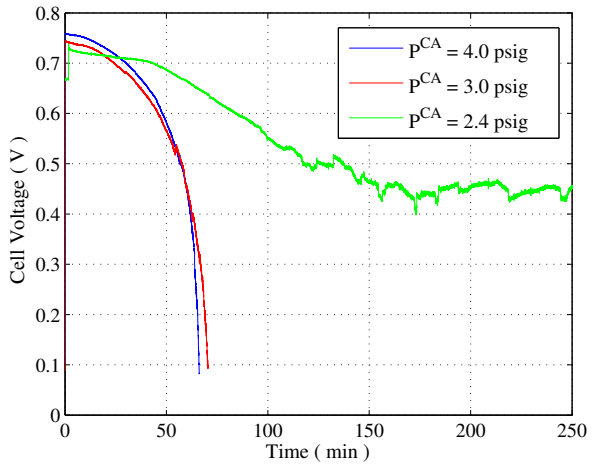

Fig. 5. The voltage evolutions toward equilibrium with three different cathode pressures. The other operating conditions are 65°C cell temperature, 60% cathode supply RH, 4.0 psig anode pressure and 0.2 A/cm^2 current density.

equilibrium under a certain set of operating conditions and the influences of operating conditions on the equilibrium can be predicted by ROM.

TABLE II
PARAMETER VALUES IN THE ROM

Quantity	Value	Unit
D_{H_2/N_2}	1.31	cm^2 s^{-1}
K_{N_2}	0.96×10^{-15}	mol Pa^{-1}m^{-1}s^{-1}
w_{ch}	2.08	mm
w_{lnd}	0.838	mm
h_{an}	1.78	mm
L_{ch}	68.5	mm
δ_{mb}	25	μm
I	10	A
A	50	cm^2
T	338	K
β_{H_2}	0.5	

The fundamental assumption in developing the ROM is the following: the evolution of N_2 blanketing front is crucial to determine the power output characteristics under a DEA equilibrium. In other words, we anticipate that a ROM that tracks the N_2 blanketing, or H_2 starvation, front can predict the power under equilibrium and influences from several key operating parameters with sufficient accuracy. The governing equation of N_2 transport is the basis of the ROM in order to track the blanketing front. The following equation of $P_{N_2}^{AN}$ comes from the FOM and holds from the inlet to the end (L_{ch}):

$$\frac{\partial P_{N_2}^{AN}}{\partial t} = \frac{\partial}{\partial y}(D_{N_2}\frac{\partial P_{N_2}^{AN}}{\partial y} - P_{N_2}^{AN}v) + \frac{K_{N_2}RT(w_{ch}+w_{lnd})(P_{N_2}^{CA}-P_{N_2}^{AN})}{\delta_{mb}h_{an}w_{ch}} \quad (4)$$

in which $P_{N_2}^{CA}$ is the N_2 partial pressure in the cathode in Pa, D_{N_2} is the Fickian diffusivity of N_2 in m^2 s^{-1}, v is the gas mixture velocity in m s^{-1}, K_{N_2} is the N_2 permeation coefficient in mol Pa^{-1} m^{-1} s^{-1}, δ_{mb} is the membrane thickness, h_{an} is the anode channel height, and w_{ch}/w_{lnd} is the anode channel/land width. The first term in the RHS of (4) represents the diffusive transport and the second one represents the convective transport. The third term is the source term capturing the N_2 crossover through the membrane depending on the local differential pressure of N_2 between anode and cathode.

The boundary conditions for (4) are zero flux at both ends, i.e., $\frac{\partial P_{N_2}^{AN}}{\partial y}$=0 at y=0 and y=$L_{ch}$; since there is no N_2 flux entering the inlet and leaving the outlet of the anode.

The state equation of H_2 is also needed for deriving a functional dependence of the convective velocity of gas mixture, v(y,t), on $P_{N_2}^{AN}$:

$$\frac{\partial P_{H_2}^{AN}}{\partial t} = \frac{\partial}{\partial y}(D_{H_2}\frac{\partial P_{H_2}^{AN}}{\partial y} - P_{H_2}^{AN}v) - \frac{iRT(w_{ch}+w_{lnd})}{2Fh_{an}w_{ch}} \quad (5)$$

in which i(y,t) denotes the local current density in A/cm^2. For simplicity, a saturated anode channel condition is assumed. Therefore,

$$P_{H_2}^{AN} + P_{N_2}^{AN} = P^{AN} - P_{sat} = P_{tot} \quad (6)$$

The total anode pressure is fixed, therefore the time derivative of (6) is zero, and the summation of (4) and (5) yields:

$$P_{tot}\frac{\partial v}{\partial y} = \frac{RT(w_{ch}+w_{lnd})}{h_{an}w_{ch}}\left(\frac{K_{N_2}(P_{N_2}^{CA}-P_{N_2}^{AN})}{\delta_{mb}} - \frac{i}{2F}\right) \quad (7)$$

During the DEA operation, the outlet velocity is zero. Therefore $v(t,L)=0$.

The local current density at the anode (H_2 dissociation) can be also described by the Butler-Volmer equation:

$$i(y,t) = i_0\left(P_{H_2}^{AN}\right)^{\beta_{H_2}}\left[\exp\left(\frac{\alpha\eta}{RT}\right) - \exp\left(-\frac{\alpha\eta}{RT}\right)\right] \quad (8)$$

in which i_0 is a lumped parameter showing the effects from all pre-multiplier constants in the Butler-Volmer equation. It is assumed that the local over-potential η is independent of the local H_2 concentration, i.e., η is a constant along the channel. Then using (3) to eliminate the exponential term in the Butler-Volmer equation yields the following expression for i(y,t):

$$i(y,t) = \frac{L_{ch}I\left(P_{tot}-P_{N_2}^{AN}\right)^{\beta_{H_2}}}{A\int_0^{L_{ch}}\left(P_{tot}-P_{N_2}^{AN}\right)^{\beta_{H_2}}dy} \quad (9)$$

in which I/A (current/area) gives the average current density in A/cm^2. The functional dependence of i(y,t) on the local N_2 concentration is important, as the cell voltage can be further estimated with sufficient accuracy in the ROM. Equations (4), (7) and (9) constitute the ROM. The parameter

values in the ROM are summarized in Table II. The ROM is solved by Comsol Multiphysics with a mesh size of 0.7 mm and relative tolerance of $1e^{-4}$.

Several assumptions are made in the ROM. First, $P_{N_2}^{CA}$ is assumed to be constant along the cathode channel given the high stoichiometry ratio in the cathode, namely, the small drop of N_2 partial pressure along the channel (about 5%) is neglected. Second, the membrane permeation coefficient K_{N_2} is assumed to be constant since the state of membrane water content is not included in the ROM. Finally, D_{N_2} is assumed to be constant along the channel. The effect of liquid water on diffusivity is neglected. The assumptions in the ROM are compared with the FOM simulations in Fig. 6. In the upper subplot of Fig. 6, the non-monotonic distribution of $P_{N_2}^{CA}$ comes from a combined effect of local oxygen/vapor partial pressure determined by local current. Since the cathode pressure is maintained constant, the decreasing oxygen partial pressure along the channel tends to produce monotonically increasing partial pressure of nitrogen, whereas the increasing vapor partial pressure leads to an opposite trend. The turning point in the subplot for $P_{N_2}^{CA}$ indicates the location where the effect of vapor pressure becomes less dominant as it approaches the saturation pressure. In the lower subplot of Fig. 6, the K_{N_2} of ROM is larger than that of FOM in order to match the rate of N_2 accumulation in the FOM, which is consistent with the prior assumption of saturated anode channel.

A comparison of the ROM predictions based on these assumptions against the actual parameter values by the FOM simulation is presented in Figs. 7 and 8. The evolutions of $P_{N_2}^{AN}$ from both FOM and ROM are shown in Fig. 7. An equilibrium has been achieved since the changes after t=5000 s are slight in both FOM and ROM, with a nitrogen blanketing front at approximately 0.6 fractional channel location. The ROM can not only predict the N_2 distribution under equilibrium, but also capture the evolution toward equilibrium accurately since the N_2 distributions at selected times are very close from both models.

Fig. 8 presents the evolutions of local current from both models. The ROM predicts a monotonically decreasing local current along the channel whereas the FOM demonstrates the non-monotonic spatial variation of local current. Since the ROM assumes constant membrane state along the channel and the local current depends only the local H_2 concentration, it cannot capture the non-monotonic local current distribution due to a combined effect from membrane self-humidification by the reaction generated water and hydrogen depletion along the channel. The FOM is capable to predict the non-homogeneity with additional membrane states.

IV. Parametric Sensitivity

We have shown that the ROM can predict the nitrogen evolution toward an equilibrium (Fig. 7) with satisfactory accuracy against the FOM. However, this finding only shows the validity of the ROM under one set of operating conditions. It is also of interest to examine whether the parametric sensitivity of the ROM is consistent with that of experimental

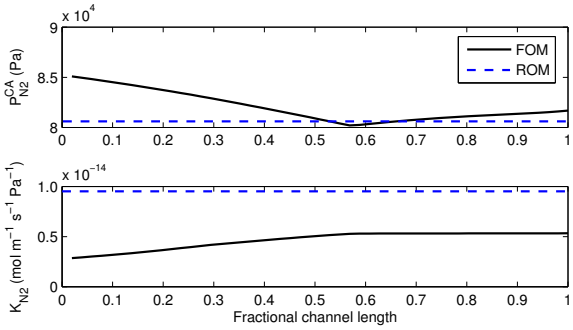

Fig. 6. The full-order-model predicted $P_{N_2}^{CA}$ and K_{N_2} under equilibrium and their values in the reduced-order-model under assumption. The operating conditions are 65°C cell temperature, 60% cathode supply RH, 4.0/2.4 psig anode/cathode pressure, 2.5 cathode SR, and 0.2 A/cm^2 current density.

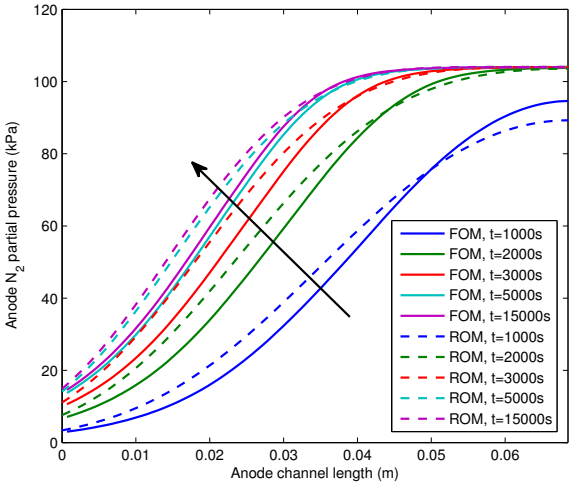

Fig. 7. The full-order-model and reduced-order-model predicted evolution of anode N_2 partial pressure toward equilibrium with the same operating conditions as in Fig. 6.

data. Cathode pressure is chosen to perform this parametric study.

Fig. 9 presents the distributions of nitrogen partial pressure and local current density under equilibrium from the ROM simulations with increasing cathode pressures. The upper subplot shows that more channel region becomes blanketed as the cathode pressure increases. Correspondingly, the local current density in the non-blanketing region increases dramatically as shown in the lower subplot. When P^{CA} increases to 4.0 psig, the local current density can exceed three times the average current density, which leads to high local water generation rate and tends to shutdown the cell. These findings are consistent with the experimental observations shown in Fig. 5 in which an equilibrium with reasonable power output (anode channel partially blanketed by N_2) was not found for higher cathode pressures.

V. Conclusions

The evolution of the nitrogen blanketing front and subsequent equilibrium in dead-ended anode operation of a

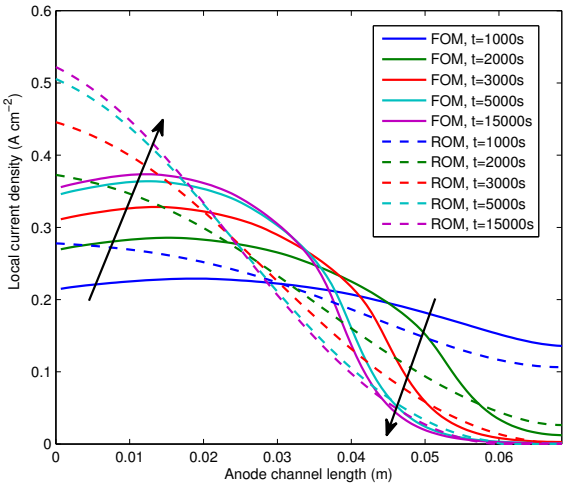

Fig. 8. The full-order-model and reduced-order-model predicted evolution of local current density toward equilibrium with the same operating conditions as in Fig. 6.

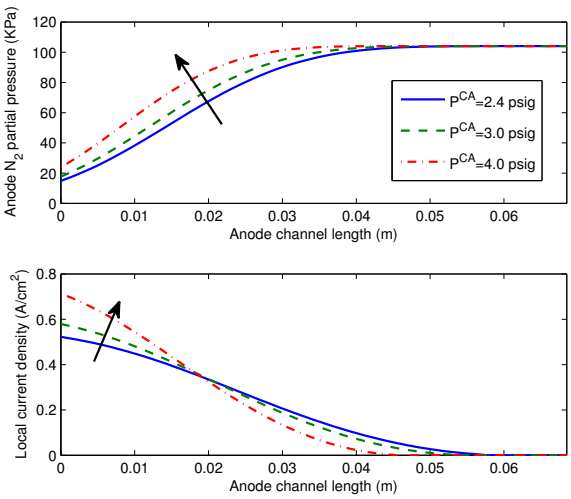

Fig. 9. The reduced-order-model and full-order-model predicted anode N_2 partial pressure and local current density distribution at equilibrium with increasing cathode pressures from 2.4, 3.0 to 4.0 psig. The other operating conditions are the same as those in Fig. 6.

fuel cell is shown to depend on the nitrogen distribution in the anode channel. The equilibrium mechanism can be summarized as zero net flux of nitrogen crossover through the membrane. For a wide range of cathode pressure, the simulation results from the tuned full-order-model (FOM) match the experimental data with satisfactory accuracy. Both FOM simulation and experimental data indicate the existence of such equilibrium, represented by voltage evolution toward a steady state, under certain operating conditions.

An assumption for the functional dependence of local current density on the N_2 partial pressure in the anode is used to calculate the convective velocity. This enables the formulation of a simplified single-state second order PDE system to study the equilibrium behavior under DEA operation. The reduced-order-model (ROM) can predict the evolution of N_2 partial pressure toward equilibrium with satisfactory accuracy as compared with the FOM. It also can capture the influences of cathode pressure on the distributions of nitrogen and local current density under equilibrium, indicating a consistent trend with the experimental data. In the future, the assumption of uniform cathode over-potential will be relaxed and a distributed voltage model will be incorporated into the ROM framework thus enabling comparison with the equilibrium voltage data from the experiments.

REFERENCES

[1] P. Mocoteguy, F. Druart, Y. Bultel, S. Besse, and A. Rakotondrainibe, "Monodimensional modeling and experimental study of the dynamic behavior of proton exchange membrane fuel cell stack operating in dead-end mode," *Journal of Power Sources*, vol. 167, pp. 349–357, 2007.

[2] D. McKay, J. Siegel, W. Ott, and A. Stefanopoulou, "Parameterization and prediction of temporal fuel cell voltage behavior during flooding and drying conditions," *Journal of Power Sources*, vol. 178, pp. 207–222, 2008.

[3] J. Siegel, D. McKay, A. Stefanopoulou, D. Hussey, and D. Jacobson, "Measurement of liquid water accumulation in a PEMFC with dead-ended anode," *Journal of Electrochemical Society*, vol. 155, pp. B1168–B1178, 2008.

[4] C. A. Ramos-Paja, C. Bordons, A. Romero, R. Giral, and L. Martnez-Salamero, "Minimum fuel consumption strategy for PEM fuel cells," *IEEE Transactions on Industrial Electronics*, vol. 56, pp. 685–696, 2009.

[5] T. Matsuura, J. Siegel, J. Chen, and A. Stefanopoulou, "Multiple degradation phenomena in polymer electrolyte fuel cell operation with dead-ended anode," *Proceeding of ASME 2011 5th International Conference on Energy Sustainability & 9th Fuel Cell Science, Engineering and Technology Conference*, Washington D.C., 2011.

[6] S. Hikita, F. Nakatani, K. Yamane, and Y. Takagi, "Power-generation characteristics of hydrogen fuel cell with dead-end system," *JSAE Review*, vol. 23, pp. 177–182, 2002.

[7] J. Chen, J. B. Siegel, and A. G. Stefanopoulou, "Nitrogen blanketing front equilibria in dead end anode fuel cell operation," in *American Control Conference*, San Francisco, CA, 2011.

[8] A. Manokaran, S. Pushpavanam, P. Sridhar, and S. Pitchumani, "Experimental analysis of spatio-temporal behavior of anodic dead-end mode operated polymer electrolyte fuel cell," *Journal of Power Sources*, vol. 196, pp. 9931–9938, 2011.

[9] E. Muller, F. Kolb, L. Guzzella, A. Stefanopoulou, and D. McKay, "Correlating nitrogen accumulation with temporal fuel cell performance," *Journal of Fuel Cell Science and Technology*, vol. 7, pp. 021 013–1–021 013–11, 2010.

[10] J. Siegel, S. Bohac, A. Stefanopoulou, and S. Yesilyurt, "Nitrogen front evolution in purged polymer electrolyte membrane fuel cell with dead-ended anode," *Journal of Electrochemical Society*, vol. 157, pp. B1081–B1093, 2010.

[11] J. Chen, J. B. Siegel, T. Matsuura, and A. G. Stefanopoulou, "Carbon corrosion in PEM fuel cell dead-ended anode operations," *Journal of Electrochemical Society*, vol. 158, pp. B1164–B1174, 2011.

[12] J. Chen, J. B. Siegel, A. G. Stefanopoulou, and J. R. Waldecker, "Optimization of purge cycle for dead-ended anode fuel cell operation," *International Journal of Hydrogen Energy*, vol. 38, pp. 5092–5105, 2013.

[13] J. F. Moxley, S. Tulyani, and J. B. Benziger, "Steady-state multiplicity in the autohumidification polymer electrolyte membrane fuel cell," *Chemical Engineering Science*, vol. 58, pp. 4705–4708, 2003.

[14] J. Benziger, E. Chia, E. Karnas, J. Moxley, C. Teuscher, and I. Kevrekidis, "The stirred tank reactor polymer electrolyte membrane fuel cell," *AIChE Journal*, vol. 50, pp. 1889–1990, 2004.

[15] W. Hogarth and J. Benziger, "Operation of polymer electrolyte membrane fuel cells with dry feeds: Design and operating strategies," *Journal of Power Sources*, vol. 159, pp. 968–978, 2006.

[16] C. Woo and J. Benziger, "PEM fuel cell current regulation by fuel feed control," *Chemical Engineering Science*, vol. 62, pp. 957–968, 2007.